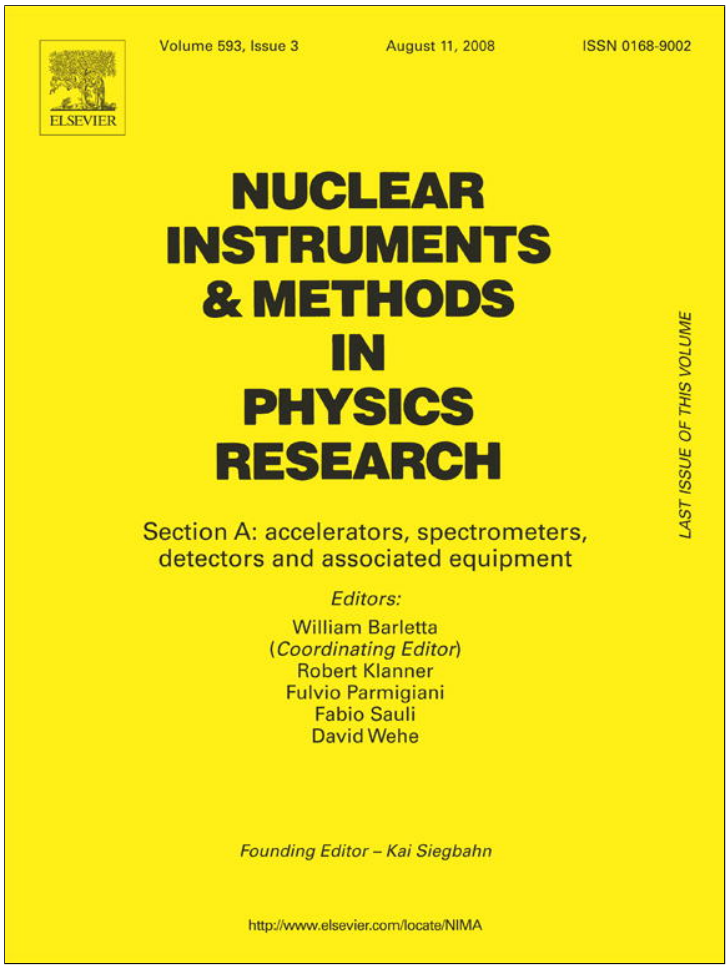

Available online at www.sciencedirect.com
ScienceDirect
Nuclear Instruments and Methods in Physics Research A 593 (2008) 188–202
NUCLEAR INSTRUMENTS & METHODS IN PHYSICS RESEARCH Section A
www.elsevier.com/locate/nima

Laser calibration system for the CERES Time Projection Chamber

Dariusz Miśkowiec[a,*], Peter Braun-Munzinger[a,b]

[a]*Gesellschaft für Schwerionenforschung mbH, Darmstadt, Germany*
[b]*Institut für Kernphysik, TU Darmstadt, Germany*

Available online 4 March 2008

Abstract

A Nd:YAG laser was used to simulate charged particle tracks at known positions in the CERES Time Projection Chamber at the CERN SPS. The system was primarily developed to study the response of the readout electronics and to calibrate the electron drift velocity. Further applications were the determination of the gating grid transparency, the chamber position calibration, and long-term monitoring of drift properties of the gas in the detector.

PACS: 29.40.Cs; 29.40.Gx

Keywords: TPC; Laser

1. Introduction

UV lasers have been widely used to simulate charged particle tracks in gaseous detectors [1–4]. Via the two-photon absorption mechanism the laser beam ionizes impurities in the gas and produces a signal which, with proper adjustment of the intensity, imitates that of a straight particle track. Large drift chambers at LEP [5–7] and at the SPS [8] made extensive use of this method. Similarly, the large cylindrical Time Projection Chamber (TPC) [9], added to the setup of the CERES experiment at the CERN SPS in 1998, was equipped with a laser system for calibration and monitoring purposes. In this paper we present the layout and the components of this system, describe the procedures employed to determine the absolute position of the laser beam, and show results of the calibration.

2. Layout of the laser system

The upgraded CERES experimental setup is described in detail in Ref. [9]. A sketch of the laser system and a pictorial representation of the experimental area, with emphasis on the components pertinent to the subject of this paper, are shown in Figs. 1 and 2, respectively. A laser generates short pulses of UV light. The laser beam is brought to the accelerator beam axis, which coincides with the symmetry axis of the TPC, at a location downstream of the TPC. From there the laser beam goes upstream along the symmetry axis up to the distribution point, located 4 cm downstream of the TPC backplate. At the distribution point the beam is reflected at an angle of 90° in ϕ-direction determined by the orientation of a rotating mirror. The radial beam goes through one or more 45° partially reflecting mirrors which send the light into the TPC, parallel to its axis, through quartz windows. Fifteen azimuthal TPC sectors have two such mirrors each, giving two laser rays at the $r = 800$ and 1200 mm, both at the azimuthal center of the sector ($\phi = 0$). The 16th sector ("special sector") has seven mirrors at $\phi = 0$ at radii of 700, 800, 900, 1000, 1100, and 1200 mm, and four mirrors at $R = 1200$ mm and $\phi = \pm 5°$ and $\pm 10°$. The laser beam is monitored using position sensitive diodes placed behind the mirrors. The individual components of the system are described in the following sections.

3. Laser

A Nd:YAG laser with two frequency doublers [10] was used to generate 4 ns long pulses of $\lambda = 266$ nm light with

*Corresponding author.
E-mail address: D.Miskowiec@gsi.de (D. Miśkowiec).
URL: http://www.gsi.de/~misko (D. Miśkowiec).

0168-9002/$ - see front matter © 2008 Elsevier B.V. All rights reserved.
doi:10.1016/j.nima.2008.02.034

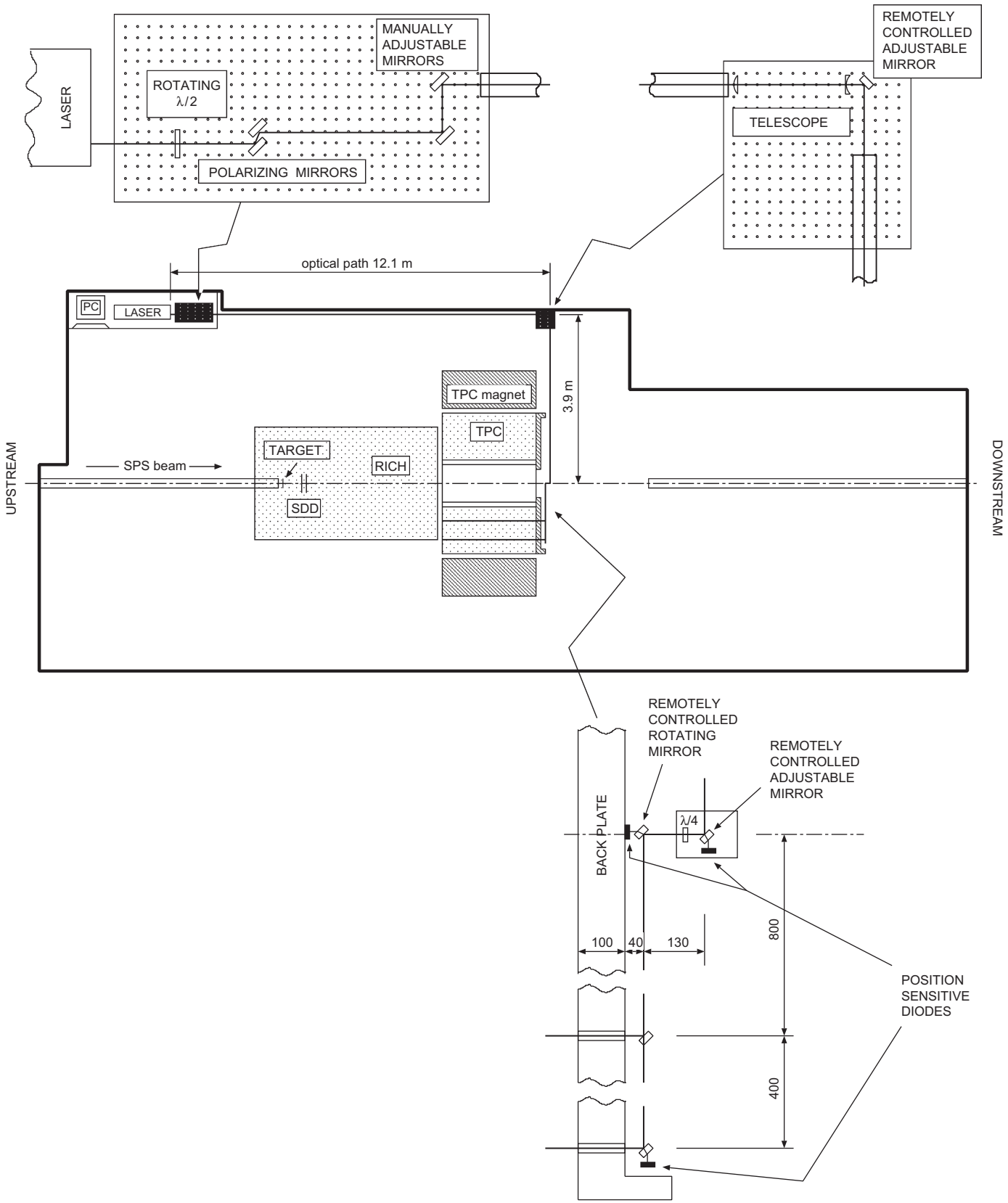

Fig. 1. Laser system layout. The laser beam travels 16 m before it arrives at the TPC. The mirrors are remotely controlled. Position sensitive diodes, placed behind the mirrors, monitor the beam position.

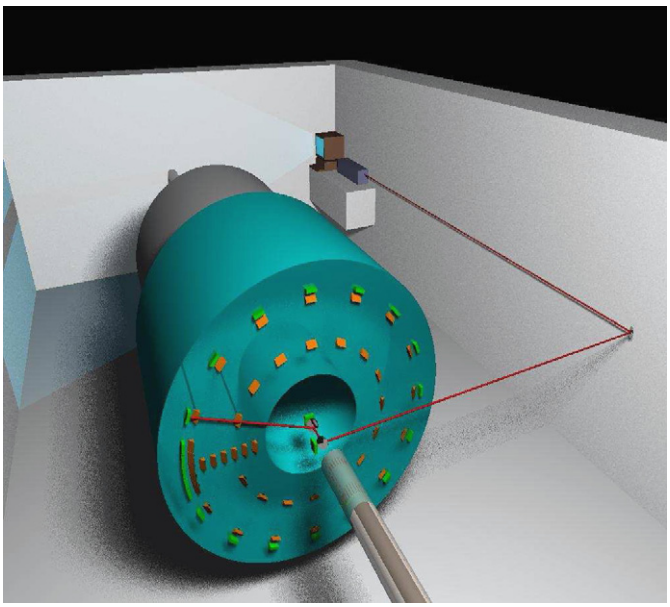

Fig. 2. Schematic view of the CERES experimental area as seen from downstream. The laser and the control PC are located in the far corner of the zone. From there the beam is transported to the distribution point where a rotating mirror sends the beam toward one of the azimuthal sectors of the TPC. Partially reflecting mirrors inject the beam into the TPC, parallel to the cylinder axis. The sector at about 9 o'clock, equipped with 11 mirrors, is referred to as "special sector".

an energy of up to 3–4 mJ per pulse and a repetition frequency of up to 10 Hz. The laser was chosen for its narrow beam and low divergence, essential for simulating particle tracks in a large drift chamber [8]. A 2 mm diameter aperture located inside the laser cavity enforced the TEM_{00} mode, resulting in a nearly Gaussian beam profile. The nominal beam diameter a (for Gaussian beams equal to 4σ) was 2 mm. The divergence, defined as the increase in diameter per unit path length in far field, was specified to be within 30% of the diffraction limit, which, for Gaussian beams, is

$$\Theta_{\mathrm{D}} = \frac{\mathrm{d}a}{\mathrm{d}z} = \frac{4\lambda}{\pi a_0}. \quad (1)$$

In the above formula Θ_{D} is the divergence angle, $a(z)$ is the beam diameter at position z, λ is the wavelength, and a_0 is the beam waist (diameter of the beam at the exit of the laser). Diffraction thus limits the product of the waist diameter and the divergence of a Gaussian 266 nm beam to be $\Theta_{\mathrm{D}} \cdot a_0 = 0.34\,\mathrm{mm} \cdot \mathrm{mr}$. Indeed, depending on the adjustment one could produce diameters of 0.8–2 mm, larger beams having smaller divergence. Under typical conditions the diameter was $a_0 = 1.2\,\mathrm{mm}$ and the divergence $\Theta_{\mathrm{D}} = 0.64\,\mathrm{mr}$, i.e. about twice the diffraction limit. A representative beam profile, measured with a laser camera [11], is shown in Fig. 3.

The primary laser beam was infrared (IR), $\lambda = 1064\,\mathrm{nm}$. Two frequency doublers converted IR to green, $\lambda = 532\,\mathrm{nm}$, and the green to UV, $\lambda = 266\,\mathrm{nm}$. The IR, the green, and the UV beams had a linear 45°, a vertical, and a horizontal polarization, respectively. Since frequency doublers convert only a part of the incident light, a prism, installed inside the laser chassis after the second doubler, was employed to separate the UV light from the other two

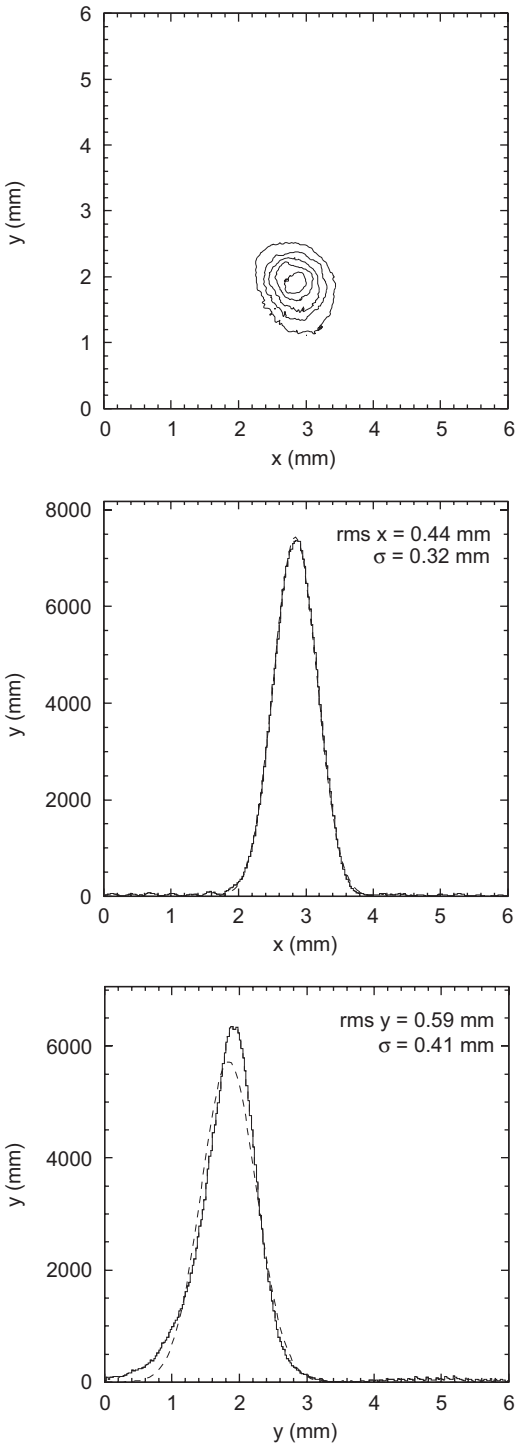

Fig. 3. The transverse intensity profile (top) of the laser beam and its two projections (middle and bottom). The standard deviations of the fitted Gaussian are $\sigma_x = 0.32\,\mathrm{mm}$ and $\sigma_y = 0.41\,\mathrm{mm}$. The measurement was done at the exit from the laser.

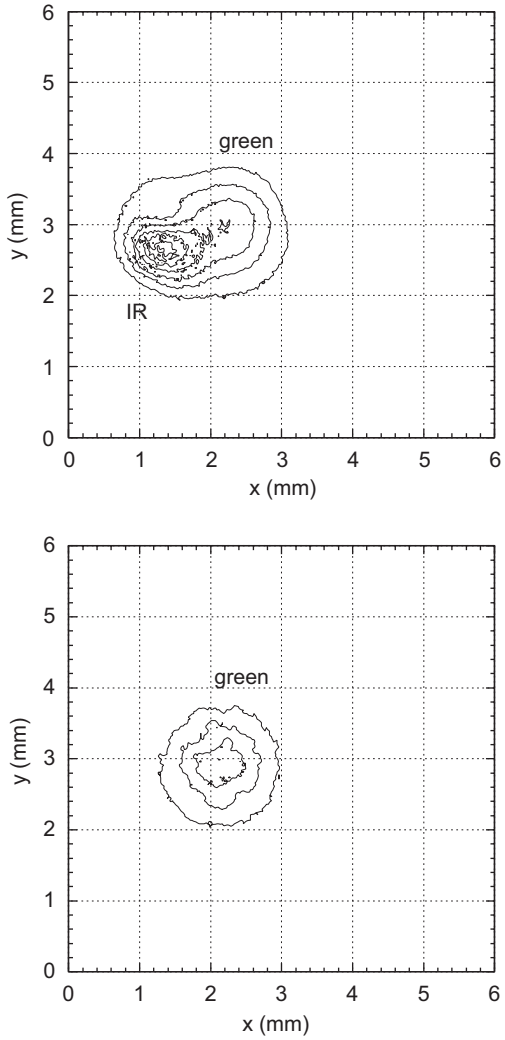

Fig. 4. Laser beam intensity profile measured with (top) and without (bottom) an IR filter in front of the camera. The IR and the green beams are obviously not aligned.

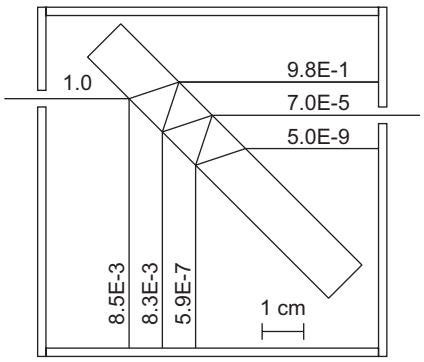

Fig. 5. Multiple reflection attenuator. The laser beam enters from the left. The attenuated beam exits through a hole in the wall. The attenuation factors were calculated using the Fresnel equations with the refraction index of quartz $n(266\,\text{nm}) = 1.4997$ and a 45° incidence angle.

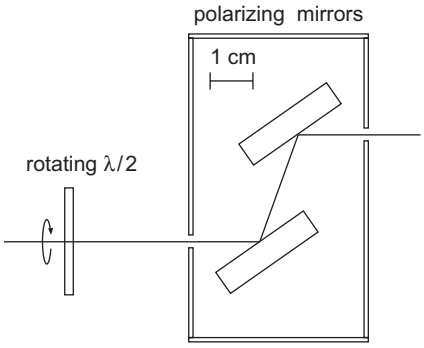

Fig. 6. Variable attenuator (top view). The laser beam goes through a $\lambda/2$ plate which, depending on its azimuthal orientation, can rotate the polarization plane of the beam. The two mirrors reflect only the vertical polarization component. This way the intensity of the outgoing beam depends on the orientation of the $\lambda/2$ plate.

wavelengths. Suppressing the unwanted wavelengths is essential since the three components are, in general, not aligned (Fig. 4) and the standard optics is usually more sensitive to green than to UV.[1]

4. Beam intensity adjustment

For many applications the laser beam needs to be attenuated. For this purpose we built a simple device based on multiple reflections in a quartz plate surrounded by black walls except for the entrance and the exit holes (Fig. 5). The attenuation factor was selected by choosing a wall with the appropriate exit hole location.

The fixed and large attenuation factors obtained using multiple reflections were of advantage during the development of the laser system components when the absolute calibration was needed. For the final setup in the experimental area a simple attenuator consisting of a rotating half-wave plate and two polarizing mirrors (Fig. 6) was used to adjust the intensity based on the TPC response. The half-wave plate rotated the polarization plane of the passing beam from its original horizontal orientation by an angle which was related to the azimuthal orientation of the half-wave plate itself. The plate was mounted in a rotary stage (Fig. 7). The rotary stage, and with it the polarization plane of the transmitted laser beam, could be adjusted remotely. The mirrors were high reflectivity (HR) coated for S-polarization, and the reflection occurred at the Brewster angle such that only the vertically polarized light survived the two reflections. The half-wave plate/mirrors combination thus provided a remotely controlled variable attenuator with the attenuation factor between 0 and 1.

Note that the laser itself provided two possibilities of adjusting the intensity: by changing the charger voltage and by changing the Q-switch delay. The first affected the flash lamp intensity. The latter changes the time elapsed between

[1]The two dichroitic mirrors employed first for this purpose were still leaving about 80 μm of IR and 30 μJ of the green light in the beam (compared to 4 mJ UV) leading to problems when measuring the beam energy or profile.

Fig. 7. Remotely controlled rotary stage [12]. The driving mechanism is based on the piezoelectric effect.

the flash and the laser action. During this time the spontaneous emission would lower the number of excited molecules and thus the longer one waited the less energy remained for the laser pulse. However, too long and too short delays resulted in high pulse-by-pulse intensity fluctuations and bad beam quality, respectively. In addition, the delay value affected the relative timing between the light pulse and the electric signal generated by the *Q*-switch electronics which was used to trigger the experiment data acquisition. For this reason we kept the delay value within 25–50% of its maximum, and adjusted the intensity by the two devices described above.

5. Beam transport from the laser to the axis of the TPC

After the polarizers the laser beam was reflected by two manually adjustable 45° mirrors. Subsequently, the beam was led out of the laser tent, located in a corner of the zone, and went about 11 m along the wall, parallel to the TPC symmetry axis and at the same height as the particle beam axis (see Figs. 1 and 2). At this point the beam reached a platform, attached to the wall, on which two lenses and a mirror were mounted. The lenses, which formed a Galilean telescope, were set up such that the beam was focused approximately 6 m from there, i.e. within the downstream half of the TPC. This location of the focus was chosen to keep the beam diameter small at the position sensitive diodes which monitor the beam position before the entrance to the TPC (see the next two sections). The transverse beam profile is shown in Fig. 8.

After passing the telescope, the beam was reflected by a 45° mirror mounted in a remotely controlled mirror holder (Fig. 9), and sent toward the symmetry axis of the TPC.

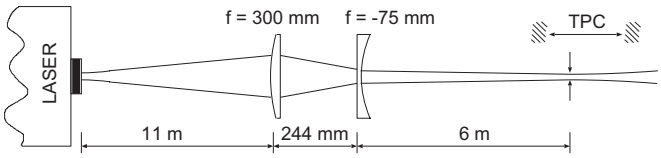

Fig. 8. Beam focusing (not to scale). At the Galilean telescope, located 11 m after the laser, the beam has a diameter of about 1 cm. The telescope focuses it back to, approximately, the initial diameter (~1 mm) inside the TPC.

Fig. 9. Remotely controlled mirror holder [13]. The three actuators can be rotated manually or by applying series of asymmetric pulses which are converted to mechanical motion via the piezoelectric effect.

6. Distribution point

The optics mounted on the TPC symmetry axis is shown in Fig. 10. The beam, which arrives horizontally from the wall of the experimental area, hits a partially reflecting mirror located on the TPC symmetry axis 17 cm downstream of the backplate (see Figs. 1 and 2). The mirror is mounted in a remotely controlled holder of the type shown in Fig. 9. The holders and the rotary stages used are driven by the piezoelectric effect and thus are not affected by a magnetic field. The transmitted beam hits a position sensitive diode. The reflected beam passes through a quarter-wave plate which transforms the linear polarization into a circular one. The advantage of the circular polarization is that the coefficients of the subsequent reflections are independent of the orientation of the rotating mirror. The rotating mirror reflects the beam radially toward one of the TPC sectors. The azimuthal angle of the mirror, and with it the sector of the TPC, can be selected remotely. Again, the mirror is semi-transparent, with a position sensitive diode placed behind it. The

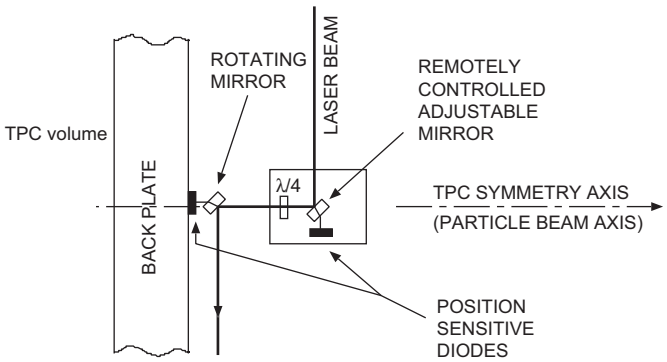

Fig. 10. Optics at the distribution point, top view.

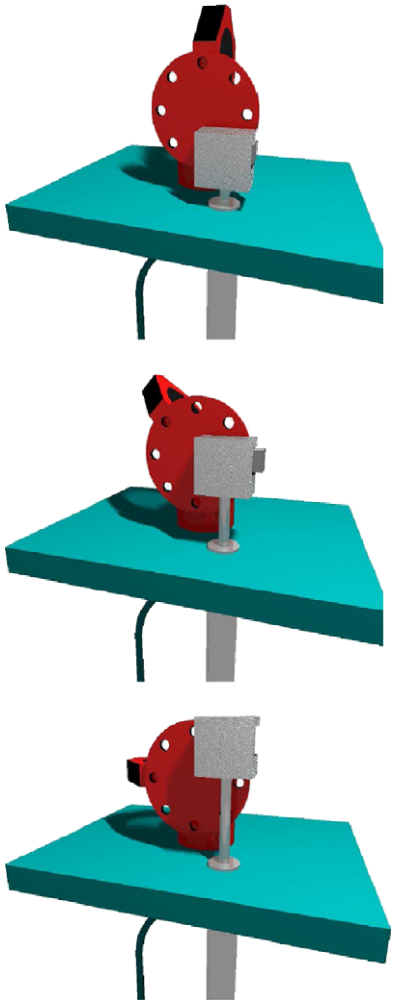

Fig. 11. Manual flipper [15] driven by a pneumatic actuator. For computer animation see Ref. [16].

reflected beam is parallel to the backplate, 4 cm from its surface.

The design, which made use of the cylindrical symmetry of the TPC, thus required that two mirrors, a diode, and a quarter-wave plate stay on the particle beam axis. Monte Carlo simulations predicted a non-negligible background in the TPC resulting from the nuclear reactions in these elements unless they were kept out during the SPS spill. Since motorized flipping mirror holders like [14] would not work because of the magnetic field we used pneumatic actuators and remotely controlled valves to move non-motorized flippers, as shown in Fig. 11. Three of the four optical elements located in the beam axis were operated as shown in this figure. The rotating mirror, however, had to be movable independently of its azimuthal orientation. The solution is shown in Fig. 12. Four pneumatic actuators were used to move an aluminum ring which pushed a hook of the central mirror holder, tilting the holder and moving the mirror out of the beam axis. In all cases the mechanics has been designed such that the final mirror positions were defined by the end-points of the holders and not by the actuators.

The pneumatic actuators were of the double acting type [18]. Two plastic tubes with an internal diameter of 2.9 mm supplied air to each of them. The air flow was regulated by PC-controlled valves. The air pressure was 2 bar and the air flow was reduced at the entrance to the cylinders for gentle operation.

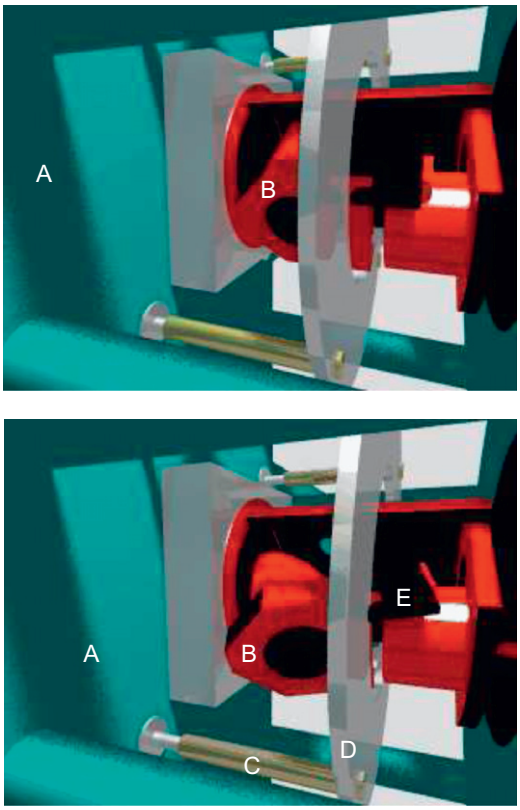

Fig. 12. Rotating mirror at the distribution point. The laser beam comes from the right and is reflected by 90° in an azimuthal direction defined by the orientation of the rotating mirror holder B, in this case (top panel) into the plane of the figure and somewhat up. For the duration of the ion beam spill the mirror is removed from the axis (bottom panel). For this, the four rods (C) driven by pneumatic actuators move the aluminum ring (D) which pushes the hook (E) of the rotating mirror holder such that the holder tilts and moves the mirror out of the beam axis, independently of its azimuthal orientation. For computer animations see Ref. [17].

The system was designed such that the mirrors would be moved into the beam at the beginning of the spill pause, the central mirror would turn toward the next TPC sector, one laser pulse would be sent with simultaneous generation of the TPC trigger, and finally the mirrors would be moved out in time for the next spill. This indeed worked at the maximum SPS energy where the spill pause was about 14 s. At 40 A GeV the spill pause was just long enough to move the mirrors in and out but not to rotate the mirror, and thus the laser events had tracks generated in just one sector of the TPC. Dedicated laser runs turned out anyway to be more useful than running in parallel with physics data taking.

Optical and acoustical inspection of the distribution point was possible by means of an ordinary black-and-white camera [19], mounted about 30 cm from the axis and connected to a TV-set in the experiment's control room.

7. Entrance to the TPC

The laser beam, reflected from the rotating mirror at the TPC axis, passed through partially reflecting mirrors which sent the rays into the TPC (Fig. 13). These mirrors were glued to massive aluminum holders, mounted on the TPC backplate with bolts. Stable geometry was essential because the laser ray position was monitored only before its entrance into the TPC, and the position inside was calculated using the calibrated mirror position and angle. The holders were calibrated in the laboratory by measuring the positions and the angles of the reflected rays as shown in Fig. 14. The reflected ray angles were measured via ray position at two different distances. The two reflection angles were first determined for each mirror holder relative to a reference holder. Subsequently, the holders were mounted in groups of four on a massive plate and the sum of the four reflection angles was measured absolutely. From the four relative and the one absolute measurement absolute reflection angles were determined for all holders. To cancel the related mounting uncertainties the measurements were repeated with different orientations of the support plate.

The TPC backplate was made of cast aluminum and had a thickness of 10 cm. The mirror holders were mounted on it with precision bolts. The exact positions of the mounting holes were measured before assembling the TPC. For this, a carousel-like custom tool and large calipers were used to determine the center of the backplate and to measure the radial positions of the mounting holes. Furthermore, mutual distances between the holes were determined. The 151 individual measurements were fit by a geometrical model with 93 free parameters, corresponding to the 90 radial r and azimuthal ϕ coordinates of the 45 holes, four unknown measurement constants, and arbitrarily fixing the

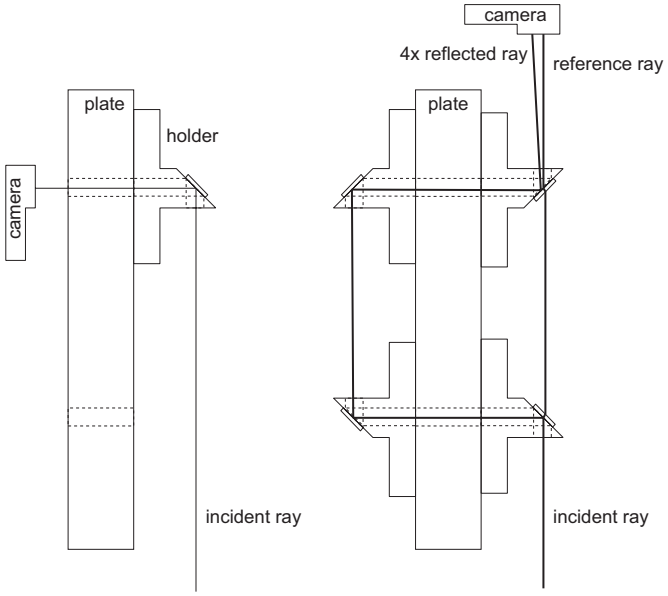

Fig. 14. Relative (left) and absolute (right) mirror angle calibration in the laboratory. The angles of the reflected rays were measured by placing the camera at two different distances.

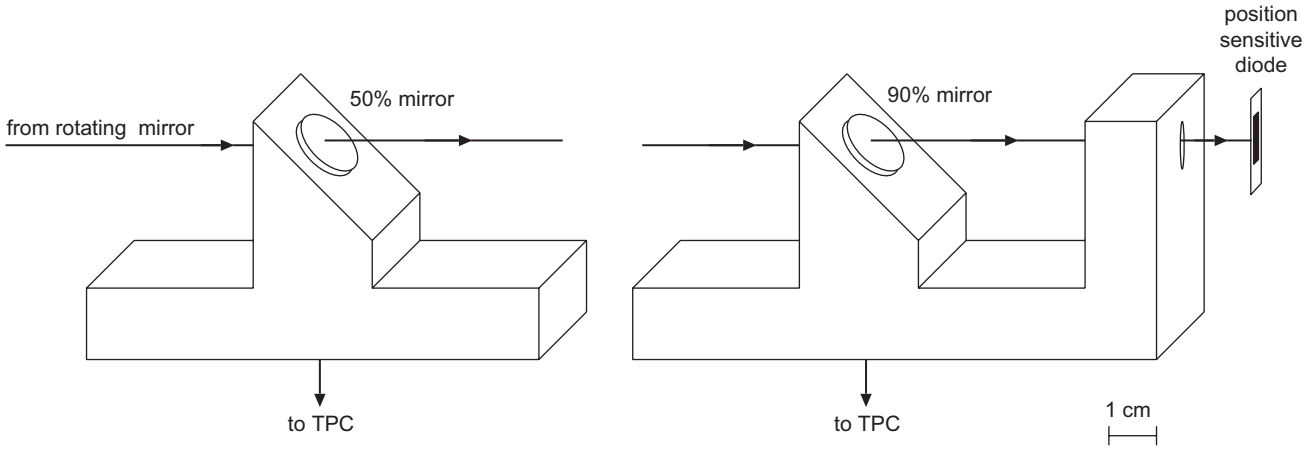

Fig. 13. Fixed mirrors which send the laser rays into TPC volume. The mirrors at $r = 800$ mm (left panel) reflect 50% of the light into the TPC. The mirror at $r = 1200$ mm (right panel) reflects 90% of the remaining light into the TPC, the rest hits the position sensitive diode.

ϕ coordinate of one hole. The chi-square of the fit allowed to estimate the precision of the obtained hole positions dr and $rd\phi$ to be 0.1 and 0.2 mm, respectively. Deviations from the design position as large as 0.5 mm, i.e. 10 times exceeding the specified limit, were observed.

As the next step, the mirror holders were mounted and the laser was turned on. The ray positions on the downstream side of the backplate were fixed using collimators. The rays emerging from the backplate on the upstream (TPC) side were measured at two distances, 3 and 30 cm. The obtained angles showed a clear correlation with the laboratory measurement of the mirror angles. Based on the width of the correlation and on the hole position uncertainties, the resolution, with which the absolute ray position inside the TPC can be calculated for a known ray position outside, was estimated to be 0.25 and 1 mm at the backplate and at the upstream end of the TPC, respectively.

The laser rays traversed the active volume of the TPC upstream parallel to the symmetry axis. At the end of their trajectory the rays would hit the upstream field cage foil. As was found in laboratory tests, 100 laser pulses with an energy of 260 μJ and a beam diameter of $a = 2$ mm were sufficient to produce a black spot on the kapton foil. With full energy (4 mJ), 600 pulses were enough to burn a hole. In order to protect the field cage, beam dumps made of ordinary microscope cover glass with a thickness of 160 μm were glued to the upstream foil at the locations corresponding to the quartz windows in the downstream foil.

8. Monitoring of the laser beam position

The calibration of the TPC was based on the assumption that the absolute position of the laser rays inside the drift chamber was known. For this, the massive backplate of the TPC was used as a reference. The geometrical calibration of the backplate and of the mirrors mounted on it was described in Section 7. Here we describe the way of monitoring the position of the laser beam with respect to these fixed elements.

The coating of the dielectric mirrors at the distribution point and of the TPC entrance mirrors at $r = 1200$ mm was chosen such that 10% of the light was transmitted. Windowless duo-lateral position sensitive diodes [20], placed behind the mirrors, were used to monitor the laser beam. The active area of the diodes was $10 \times 10\,\text{mm}^2$ and the nominal position resolution was better than 1 μm. Hit by a laser beam, each diode produced two cathode and two anode signals. The sum of amplitudes was proportional to the light intensity, and the difference between the two cathode (anode) signals was related to the horizontal (vertical) position of incidence. The coordinates were reconstructed from the measured right, left, up, and down signals r, l, u, d via

$$x = 5\,\text{mm} \cdot (r - l)/(r + l)$$

$$y = 5\,\text{mm} \cdot (u - d)/(u + d). \quad (2)$$

The signals were amplified, stretched, and digitized by electronics located on two $10 \times 10\,\text{cm}^2$ large boards [21]. The diode itself was mounted on the first board (Fig. 15). Precision bolts ensured exact positioning of the mounted boards. The boards were connected via a daisy chain to a PC. The readout was first triggered internally by the enabled diodes. This was later replaced by an external trigger derived from the laser Q-switch. After each event the data of all diodes were transported to the memory of the PC via an interface connected to the parallel port.

The linearity and the resolution of the diodes were tested in laboratory by illuminating each diode at 81 positions on a 1 mm grid (Fig. 16). For this, each diode in turn was mounted on a pair of computer-controlled linear stages. The calibration procedure was fully automatic and consisted in shifting the diode to each of the 81 positions, switching on the laser, and recording 100 diode events. The typical resolution of a single spot was $\sigma_x \approx \sigma_y \approx 30\,\mu\text{m}$. The global resolution after the calibration was about 50 μm. The laser beam energy during such a measurement was typically 1 μJ.

The second batch of the diodes delivered turned out to require as much as 10 μJ in order to achieve a good resolution. These diodes were assigned to the locations at which the intensity of the incident laser beam was higher.

One of the diodes was placed on the rotating mirror holder, with the connections to the readout electronics provided via four sliding pins, and used to monitor the position of the reflected beam. A dedicated semi-transparent mirror, placed on the laser beam right after the rotating mirror, was reflecting a small fraction of the laser light onto this diode. (For simplicity these two elements were left out

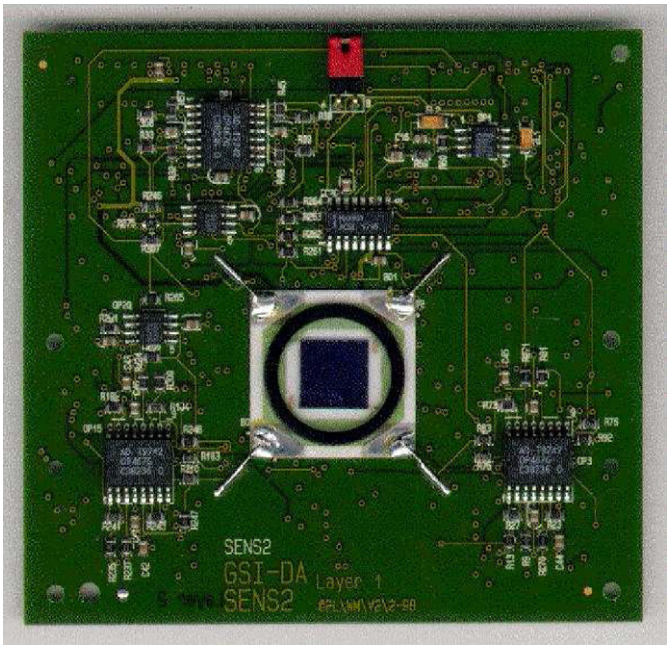

Fig. 15. Position sensitive diode [20] on the readout board [21].

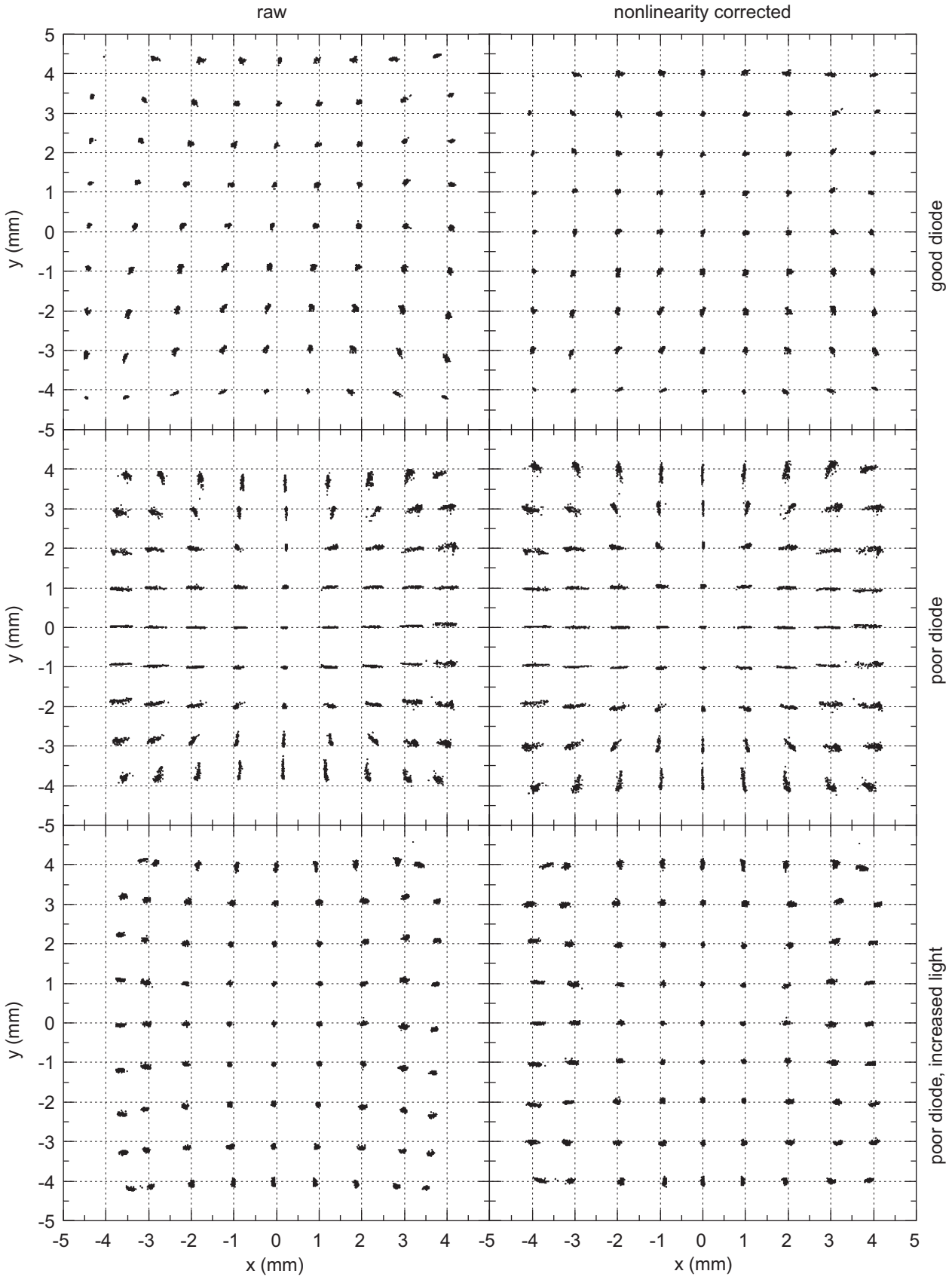

Fig. 16. Laser beam position recorded during a scan of the position sensitive diodes, raw (left) and after calibration (right). The uppermost row shows a good diode from the first production batch. Diodes from the second batch showed a much worse resolution (middle row) but recovered when illuminated with a higher light intensity (bottom row).

in Fig. 10.) During a rotation of the mirror the spot on this diode would follow a circle whose radius would indicate the deviation of the laser beam from the mirror rotation axis and thus from the symmetry axis of the TPC. An example is shown in the bottom panel of Fig. 17. The upper panel of the same figure shows the position of the transmitted ray, displaced after having traversed the 6 mm thick mirror at an incidence angle of 45°. The information from this diode was used to monitor the mirror angle during the rotation. The correction necessary to bring the beam to the axis could be calculated from the data collected by these two diodes during a 2π rotation, combined with the z-coordinates of the reflected beam measured on the diodes distributed on the circumference of the TPC. This procedure could be applied iteratively; in praxis, one iteration was sufficient to place the incident beam exactly (better than 100 μm) on the TPC symmetry axis.

After the incident beam was placed on the axis, the position information from all diodes, combined with the known reflection angle of the mirror at the entrance to the TPC, was used to calculate the laser beam position in the TPC. This, in principle, could be done separately for each single laser event. However, with the excellent laser pointing stability (standard deviation at the entrance to the TPC of 60 μm) within the duration of a typical laser run (10 min), it was more convenient to use the average beam position of a run. This information, combined with the knowledge of the mirror geometry, was used to determine the laser track positions in the chamber.

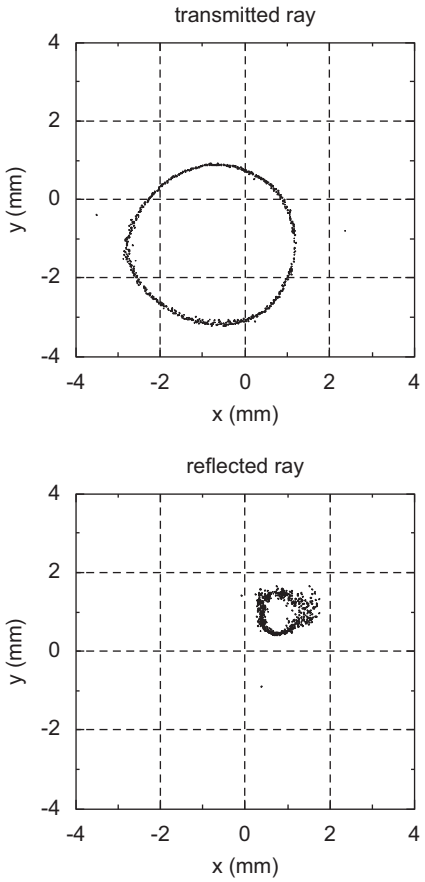

Fig. 17. Position of the laser beam transmitted through (up) and reflected by (bottom) the rotating mirror. The finite radius of the upper circle results from the finite thickness of the mirror. The lower circle shows that the laser beam is not on the rotation axis. See text for details.

9. Computer control

A personal computer running under Linux was used to control the laser and the optomechanics, and to collect the diode data. Synchronization with the accelerator spill signal was achieved via an I/O card. The same I/O card was used to control the air valves of the actuators for moving mirrors in and out of the beam axis, described in Section 6. The logical scheme is shown in Fig. 18. In laboratory tests the PC was used to read the CCD camera and to perform fully automatic diode scans involving moving linear stages, switching the laser, and collecting diode data.

10. Trigger timing

While in nuclear collision events the data acquisition trigger was generated using the incident beam particle, for laser events the trigger was derived from the Q-switch of the laser. The timings of these two triggers were not identical. The time difference was determined in two ways. First, during a dedicated test a 0.5 mm diameter light guide was used to connect the laser with a scintillator located some 5 m downstream of the TPC such that the attached phototube was seeing a scintillation signal in collision

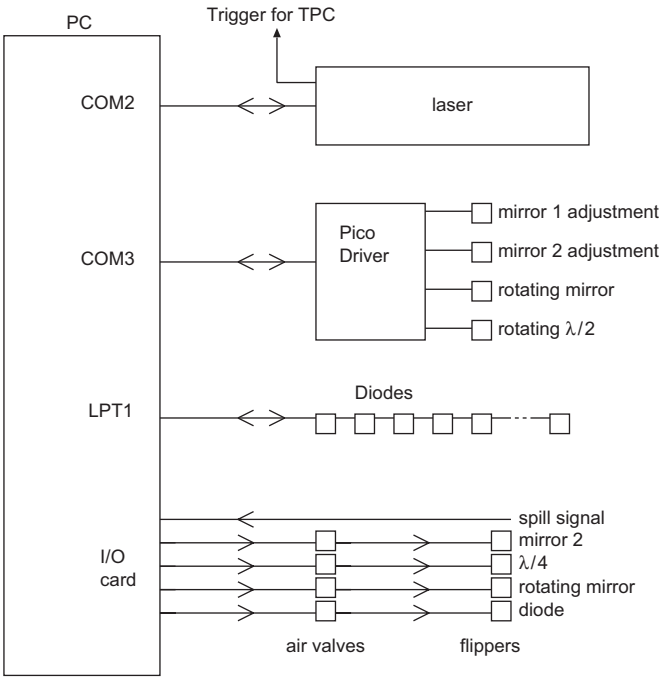

Fig. 18. Control computer connection scheme.

events and laser light in laser events. After correcting for the time-of-flight of particles and for the light propagation velocity in the light guide, in a separate test determined to be 19.4 cm/ns, the time difference between the two triggers was calculated to be between 300 and 410 ns, depending on the laser settings, to be subtracted from the TPC drift times in laser events before they can be compared to nuclear collision events. The estimated accuracy of this measurement was 20 ns. The result was in good agreement with the number obtained by the second method which consisted in comparing the position of the peak caused by photoelectrons from the high voltage cylinder limiting the drift volume at low radii (see Section 11), seen in laser events, with the edge of the radial distribution of hits in collision events.

11. TPC commissioning with laser

First laser tests of the TPC were performed in May 1998. The laser beam was sent into the special sector of the TPC. Every laser pulse produced seven parallel tracks at the same ϕ and at different radii. The response of two pads of the readout chamber is shown in Fig. 19.

In summer and fall of 1998 the TPC was fully equipped with readout electronics and various calibrations were performed with tagged muons and the laser. A typical laser event from that time is shown in Fig. 20. In addition to the tracks made by laser rays ionizing TPC gas the signal from the high voltage cylinder is visible, generated by photoelectrons from the aluminum (work function 4.28 eV) produced by scattered laser photons ($\hbar\omega = 4.65$ eV). Close to the TPC ends the reconstructed tracks exhibit curvature indicating a

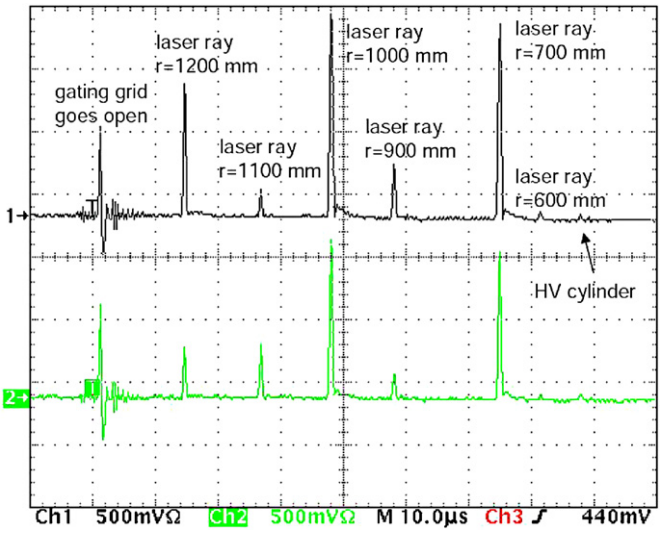

Fig. 19. Charge on two readout pads versus drift time. The bipolar pulse is due to switching of the gating grid. The peaks are caused by laser rays. Some of the laser rays are not properly centered and thus have a lower intensity. The ray at $r = 800$ mm is not visible at all. The tiny peak on the right-hand side (longest drift time) represents photoelectrons produced on the high voltage cylinder by the scattered laser light.

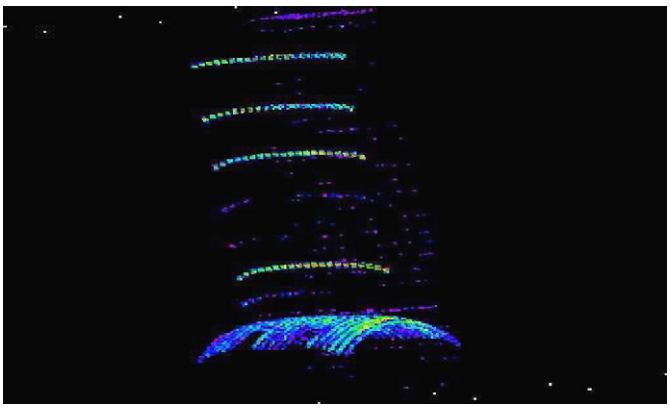

Fig. 20. Laser tracks reconstructed in the first tests in the special sector of the TPC.

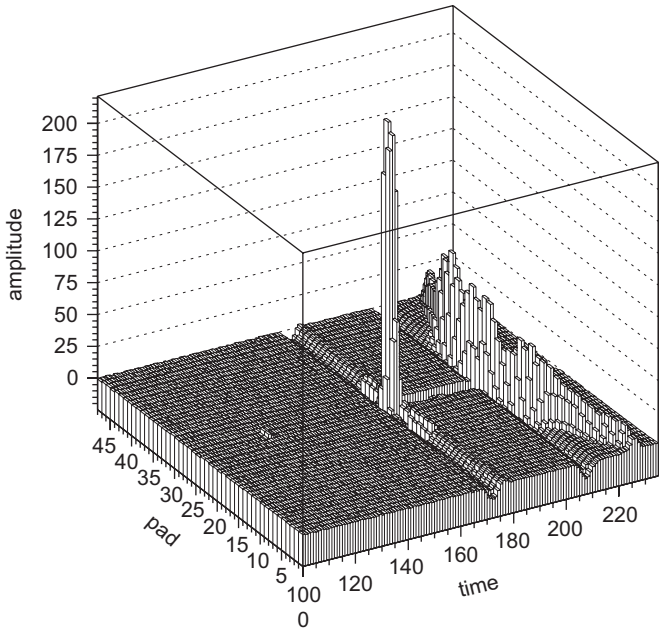

Fig. 21. Response of a readout chamber averaged over many laser events. The laser pulse is accompanied by an undershoot and the lateral cross-talk. The signal at high drift times, distributed over many pads, comes from photoelectrons knocked out of the high voltage cylinder by the scattered laser photons.

z-dependence of the electric field not accounted for by the reconstruction software. This observation triggered a new three-dimensional calculation of the electric field [9].

12. Pulse shape and grid transparency studies

The laser system allows to generate many events with a track at the same position and with similar signal amplitudes. By averaging over many events in the absence of other tracks details of the pulse shape of the readout chamber can be studied. Two effects of interest, an undershoot following each pulse and a negative signal on pads coupling to the same anode wire (“lateral cross-talk”) are shown in Fig. 21 (taken from [22]). Also visible is the

signal coming from electrons knocked out of the high voltage cylinder by stray laser light. The shape of the undershoot has been parametrized and corrected for. The possibility of accurately adjusting the laser beam intensity proved helpful in studying these subtle effects.

Ions produced by electrons via gas amplification in the vicinity of the anode wires were kept out of the TPC drift volume by means of a gating grid which was opened only for the duration of the drift time (70 μs) after each trigger. The wires of the gating grid had an offset potential of −140 V in the open state, matched to the electric field of the drift volume, and alternating potentials of −70 and −210 V (bias of ±70 V) in the closed state. The voltages were chosen based on a measurement of the grid transparency in laser events. The procedure is described in detail in Ref. [9].

13. Calibration of the chamber position and of the electronics time offset

The electrons knocked out of the high voltage cylinder by scattered laser light traverse the full drift volume before they hit a readout chamber. With proper calibration the reconstructed origin of the electrons should reproduce the radius of this cylinder $r = 486$ mm. This constraint was used to calibrate the length of the drift path and the pad-to-pad time offsets. In a plot of the raw drift time measured for these electrons, shown in Fig. 22, the periodic structure in ϕ, represented by the pad number, is the dominant feature. It is caused by the fact that the 16 readout chambers form a polygon around the otherwise cylindrical TPC and thus the drift path is longer for electrons arriving at the edge of a chamber. After accounting for this, the misalignment of the chambers, affecting the drift times via the path length and the electric field, becomes visible as collective shifts or tilts of groups of 48 pads (Fig. 23). Another effect manifest in the plot is a three-peak structure within each chamber caused by different capacities of the connections between the pads and the preamplifiers leading to differences in time offsets. The structure is related to three front-end-boards (group of 16 pads). Finally, individual time offsets were allowed for each front-end-board. The corrected data are shown in Fig. 24. It should be noted that a similar analysis can be

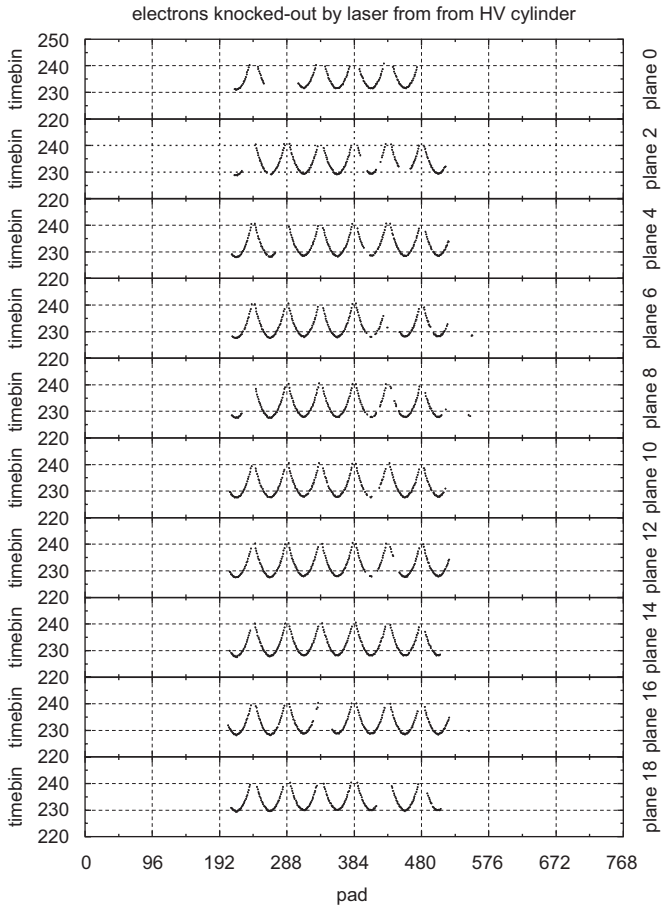

Fig. 22. The drift times of electrons emitted from the high voltage cylinder to individual pads (related to ϕ) for several readout planes (z). The periodic structure is caused by the polygonal shape of the readout. The laser illuminates the high voltage cylinder only from one side.

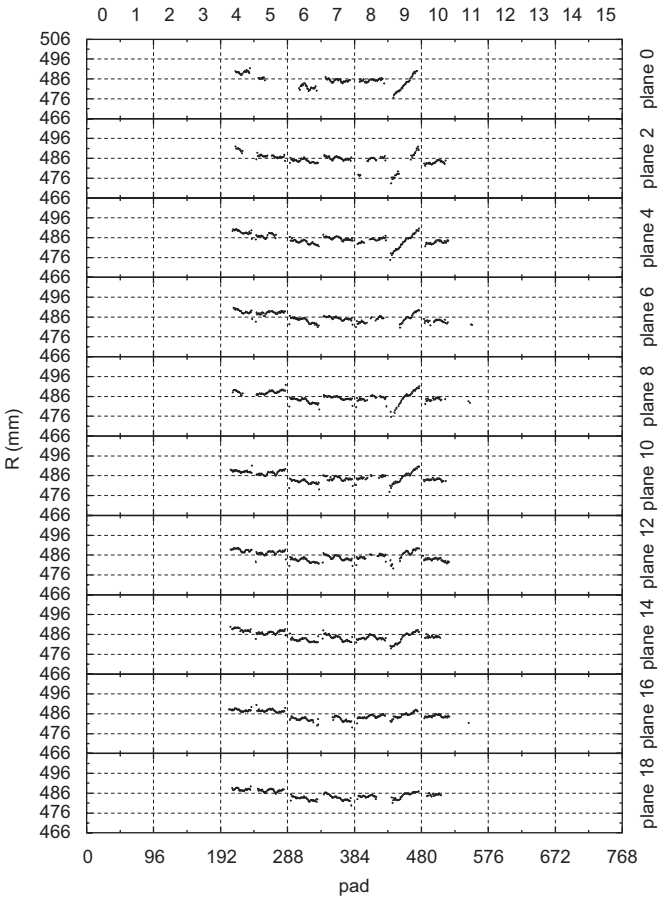

Fig. 23. Radius of the high voltage cylinder reconstructed from the drift time of the photoelectrons (comp. Fig. 22). The numbers at the top indicate the 16 readout chambers, 48 pads each. The structures caused by misaligned readout chambers and a periodic distortion within each chamber, related to three front-end-boards, are visible.

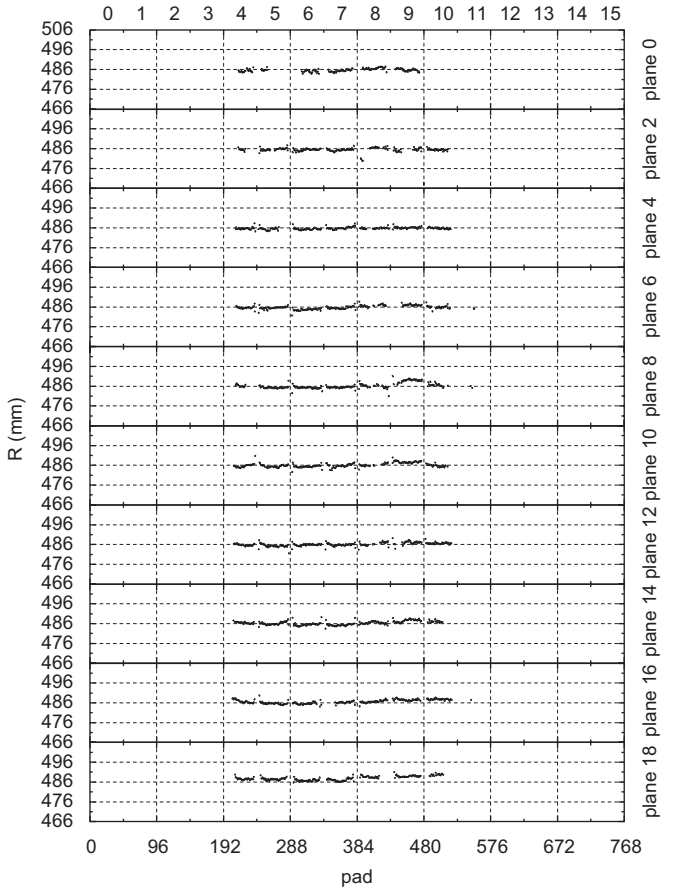

Fig. 24. Reconstructed radius of the high voltage cylinder after calibration.

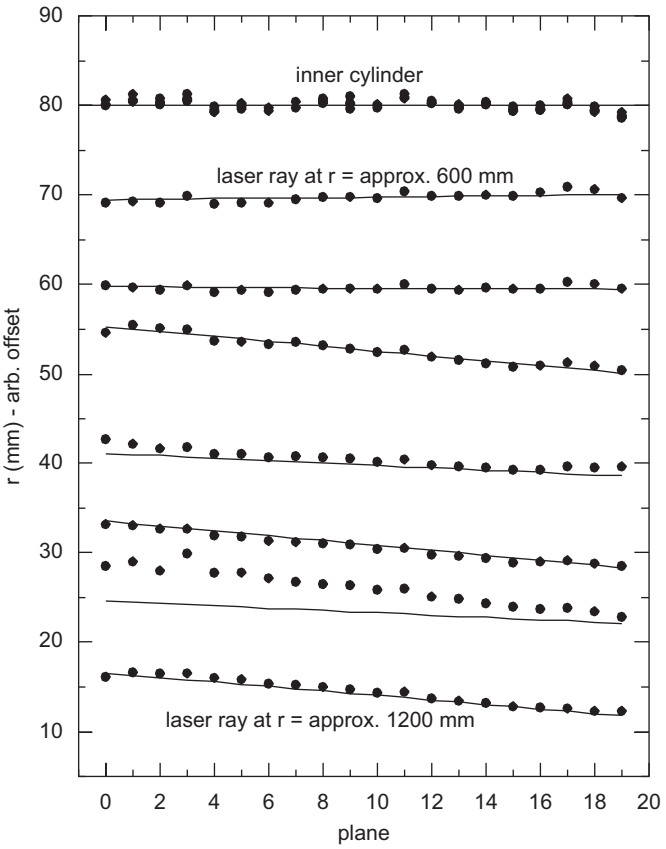

Fig. 25. Reconstructed laser tracks and the high voltage cylinder after the 12-parameter field/mobility fit. The points and the lines represent calibrated measurements of the radial hit coordinate and the expected track positions based on the diode information, respectively, for the 20 z-planes of the TPC.

performed using the edge of the time distribution collected for each pad in nuclear collision events. The calibration obtained this way matches more closely the experimental conditions during physics data taking. This way was actually used to calibrate the chamber positions and time offsets for the last CERES run in 2000. For a discussion of the resolutions achievable within these two methods see Section 15.

14. Determination of drift velocity and electric field corrections

The CERES TPC operated with an inhomogeneous electric field. The exact knowledge of the electric field on one side and of the drift velocity for different field values on the other was necessary for track reconstruction. A calibration run consisting of 1000 laser events with seven laser rays in the special sector and with the photoelectron signal from the high voltage cylinder was used to determine the electron mobility function and the electric field corrections in absence of the magnetic field. This was done by minimizing radial distances of the reconstructed TPC hits from the expected track (and cylinder) positions. The expected track positions were calculated from the laser beam position before entering the TPC, measured with the position sensitive diodes, and the known mirror positions and angles, as described in Section 7. The 12 minimization parameters included three factors for electric field corrections at each end of the TPC, five parameters of the electron mobility curve, and the time offset. (The electric field corrections were still needed to remove the remnants of the track curvature in r vs. z, visible in Fig. 20, after most of the effect was cured by taking into account the voltage dependence of the resistors in the divider chains and performing the three-dimensional potential calculation [9].)

Fig. 25 shows the result of the minimization. The tracks were approximately parallel to the beam axis at $r = 60$, 70, 80, 90, 100, 110, and 120 cm; the radius of the high voltage cylinder was 48.6 cm. For better visualization in Fig. 25 the reconstructed tracks (points) were shifted closer to each other by arbitrary offsets; the same offsets were applied to the lines denoting the expected track positions. The difference between the points and the lines shows the residual distortions in the absolute scale. The track at $r = 110$ cm, for which the mirror angle seems to deviate systematically from the assumed value, was excluded from the minimization.

In a radial drift chamber, unlike in a typical TPC where the drift occurs at a fixed value of electric field, the whole mobility curve is needed for track reconstruction. The five-parameter mobility curve obtained from the fit differed significantly from results of a calculation performed with the drift simulation package Garfield/Magboltz [23] (Fig. 15 in [9]). The laser events with tracks at known positions were thus essential for understanding of the electron drift in the CERES TPC.

15. Drift velocity monitoring

The drift time of the electrons knocked out from the high voltage cylinder in laser events can be used to monitor the changes in drift velocity with time. This mode of operation was tested during the Au + Pb run at 40 GeV per nucleon in 1999. Over several days of data taking in the pause between bursts the mirrors were flipped in and a laser event was generated. This event was becoming the first event on tape of the subsequent burst. The drift time of electrons registered in these events is shown in Fig. 26. In this figure, a period of two days is represented during which a distinct change in drift velocity occurred caused by the replacement of a gas filter. The drift times measured by four groups of two pads are represented as a scatter plot and as a profile in the left and right panel of Fig. 26, respectively. For comparison, filled dots in the right panel represent the full drift time extracted from the edge of the time distribution of hits recorded in nuclear collision events (for clarity shifted down by 20 timebins). The resolution of the laser method is 0.2 timebin (1 timebin = 294 ns) per pad per event. Properly combining one third of all pads (the laser illuminates only one side of the cylinder), i.e. $1/3 \times 16$ chambers $\times$ 20 planes $\times$ 48 pads/chamber/plane = 5120 pads, should result in a resolution on the order of 0.003 timebins per event. This is to be compared to 0.9 timebin per event achievable with the edge method.

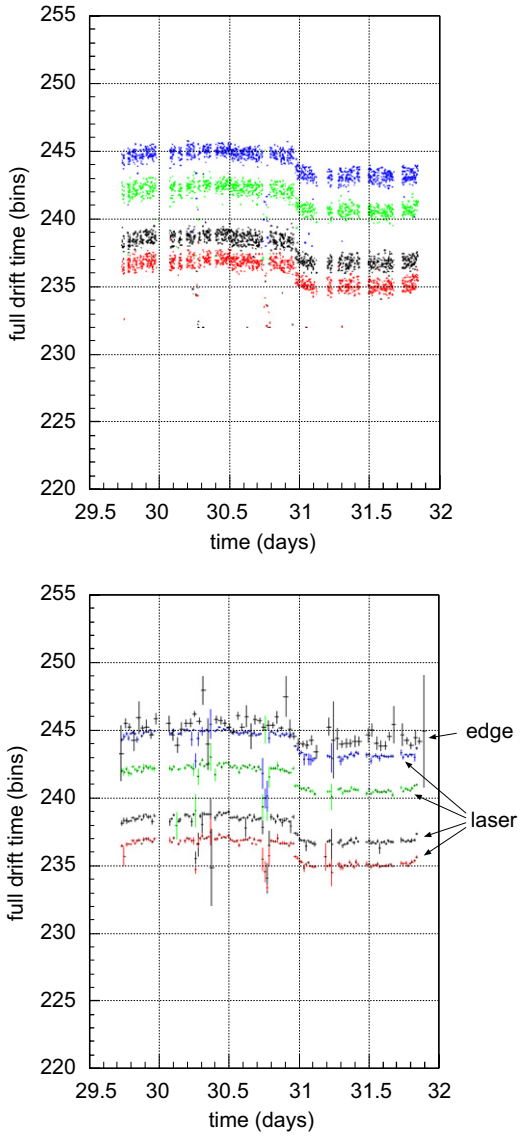

Fig. 26. Drift time of electrons from the high voltage cylinder to four groups of two pads, as a scatter plot (left panel) and a profile (lower four sets in the right panel), compared to the maximum drift time extracted from the edge of the time distribution of hits recorded in collision events (full dots in the right panel). The methods are consistently revealing the change in the drift velocity caused by a change in gas composition.

While the laser method provides a much superior measurement of the total drift time in a single event, the low rate of laser events taken in the monitoring mode and the effort needed to maintain the system stable over many days make it less practicable than the other method. The final calibration of the drift velocity was performed with nuclear collision events using the edge of the radial hit distribution.

16. Summary

The CERES TPC laser system was essential for verifying the electric field map and for understanding the electron drift in the inhomogeneous electric field, as well as for studying the detailed response of the readout chambers.

It provided, furthermore, a convenient way to determine the gating grid transparency, to calibrate the chamber positions and the pad time offsets, and, by running the laser in parallel to production runs, to monitor the drift properties of the detector. Here, however, obtaining the analogue results from the recorded collision events was more practicable.

Acknowledgments

The vigorous contribution of Wawrzyniec Prokopowicz to this project is gratefully acknowledged. We thank Peter Liebold for building and improving the diode readout and the technicians Michael Marquardt and Joachim Weinert for their perfect work. Finally, we thank Hannes Wessels and Wilrid Dubitzky for carefully reading the manuscript and spotting many (hopefully all) errors and inconsistencies.

References

[1] J.C. Guo, F.G. Hartjes, J. Konijn, Nucl. Instr. and Meth. 204 (1982) 77.
[2] J. Konijn, F.G. Hartjes, Nucl. Instr. and Meth. 217 (1983) 311.
[3] S.R. Amendolia, et al., Nucl. Instr. and Meth. A 235 (1985) 296.
[4] H.J. Hilke, Nucl. Instr. and Meth. A 252 (1986) 169.
[5] C. Brand, et al., Nucl. Instr. and Meth. A 283 (1989) 567; Y. Sacquin, Nucl. Instr. and Meth. A 323 (1992) 209.
[6] W.B. Atwood, et al., Nucl. Instr. and Meth. A 306 (1991) 446.
[7] O. Biebel, et al., Nucl. Instr. and Meth. A 320 (1992) 183.
[8] J.W. Harris, et al., Nucl. Instr. and Meth. A 315 (1992) 33; R. Renfordt, NA49 internal note NA49/LASER/96-00.
[9] G. Agakichiev, et al., Nucl. Instr. and Meth., submitted for publication, arXiv:xxxxxxx [nucl-ex].
[10] Spectron Laser Systems SL 401T Nd:YAG, Polytec, D-76337 Waldbronn.
[11] LaserCam™ CCD Camera, Coherent GmbH, D-64807 Dieburg.
[12] Motorized Rotary Stage 8401M, New Focus Inc., San Jose, CA 95134.
[13] Motorized 1″ Corner Mirror Mount 8809M, New Focus Inc., San Jose, CA 95134, Santa Clara, CA 95051-0905.
[14] Motorized flipper 8891M, New Focus Inc., San Jose, CA 95134.
[15] Flip-out mirror mount 9891M, New Focus Inc., San Jose, CA 95134.
[16] ⟨http://www.gsi.de/~misko/ceres/laser/flipper.gif⟩.
[17] ⟨http://www.gsi.de/~misko/ceres/laser/otron-rotating.gif⟩; ⟨http://www.gsi.de/~misko/ceres/laser/otron-flipping.gif⟩; ⟨http://www.gsi.de/~misko/ceres/laser/otron-flipping-and-rotating.gif⟩.
[18] DSN-8-10P and DSN-8-25P, FESTO Pneumatic AG, D-73734 Esslingen.
[19] CCD camera module 116785, Conrad Electronic GmbH, D-92240 Hirschau.
[20] Silicon Sensor DL-100-7Ker without window, Gigahertz-Optik GmbH, D-82178 Puchheim.
[21] Design by H.-P. Liebold, J. Hoffmann, GSI Darmstadt.
[22] W. Schmitz, Ph.D. Thesis, Uni Heidelberg, 2001.
[23] R. Veenhof, Nucl. Instr. and Meth. A 419 (2–3) (1998) 726; S.F. Biagi, Nucl. Instr. and Meth. A 421 (1–2) (1999) 234.